*European Cells and Materials* Vol.48 2024 (pages 1–16) DOI: 10.22203/eCM.v048a01 ISSN 1473-2262

*Original Article*

# CELLULAR RESPONSE TO SHORT-TIME MECHANICAL STIMULI: MEDIATING $Ca^{2+}$ INFLUX VIA PIEZO1

Fuan Wang[1,2,§], Hongkun Chen[1,2,§], Zhongyuan He[1,2,3,§], Jianfeng Li[1,2], Zhengya Zhu[1,2,4], Tao Tang[1,2], Junhong Li[1,2,5], Jiaxiang Zhou[6], Qiuxiao Tan[7], Zhen Li[8], Martin J. Stoddart[8], Xizhe Liu[2,*], Manman Gao[9,*], Zhiyu Zhou[1,2,*] and Shaoyu Liu[2]

[1]Department of Orthopaedic Surgery, Innovation Platform of Regeneration and Repair of Spinal Cord and Nerve Injury, The Seventh Affiliated Hospital, Sun Yat-sen University, 518107 Shenzhen, Guangdong, China
[2]Guangdong Provincial Key Laboratory of Orthopedics and Traumatology, The First Affiliated Hospital of Sun Yat-sen University, 510060 Guangzhou, Guangdong, China
[3]Department of Orthopaedics, The Second Affiliated Hospital of Chongqing Medical University, 400010 Chongqing, China
[4]Department of Orthopaedic Surgery, The Affiliated Hospital of Xuzhou Medical University, 221004 Xuzhou, Jiangsu, China
[5]Department of Orthopaedics and Trauma, The Affiliated Hospital of Yunnan University, Yunnan University, 650031 Kunming, Yunnan, China
[6]Department of Spinal Surgery, The Affiliated Hospital of Qingdao University, 266005 Qingdao, Shandong, China
[7]Department of Gynecology and Obstetrics, The Seventh Affiliated Hospital, Sun Yat-sen University, 518107 Shenzhen, Guangdong, China
[8]AO Research Institute Davos, 7270 Davos Platz, Switzerland
[9]Department of Orthopedics, Fuzhou Second Hospital, 350007 Fuzhou, Fujian, China
[§]These authors contributed equally.

**Abstract**

Physical activity shows a positive correlation with overall health, and vigorous intermittent lifestyle physical activity (VILPA) similarly offers advantages in reducing the risk of all-cause mortality. Might the short-time mechanical stimuli be discernible to cells, eliciting commensurate physiological responses? The study's objective was to investigate the cellular response to short-time mechanical stimuli. Human umbilical cord-derived mesenchymal stem cells (hUCMSCs), isolated and thoroughly characterized, were subjected to various stimuli, including activation and mechanical stretching, with $Ca^{2+}$ influx assessed through alterations in fluorescence intensity. Further validation of these findings was confirmed through short hairpin RNA (shRNA) and inhibitors. In addition, a comprehensive examination of PIEZO1 alterations was conducted through quantitative real-time polymerase chain reaction (qRT-PCR) and western blot (WB) techniques. The results shown different frequencies of stretching stimulation and durations induced varying degrees of $Ca^{2+}$ influx. The most substantial increase occurred within 2–3 minutes in the group subjected to 0.5 Hz stretching for 2 minutes ($p < 0.05$). Stretching at 0.5 Hz resulted in significant elevation in *PIEZO1* mRNA expression at 15 minutes and 1 hour. Additionally, stretching cause a gradual rise in PIEZO1 protein levels, with a notable peak observed at 2 hours. In conclusion, cells primarily sense short-time mechanical stimuli through PIEZO1, predominantly mediated by regulated $Ca^{2+}$ influx. This underscores PIEZO1's crucial role in cellular responsiveness to transient mechanical cues, advancing our understanding of mechanosensory mechanisms in cellular physiology.

**Keywords:** Vigorous intermittent lifestyle physical activity, short-time mechanical stimuli, PIEZO1, $Ca^{2+}$ influx, Yoda1.

***Address for correspondence**: Xizhe Liu, Guangdong Provincial Key Laboratory of Orthopedics and Traumatology, The First Affiliated Hospital of Sun Yat-sen University, 510060 Guangzhou, Guangdong, China. Email: liuxizhe@mail.sysu.edu.cn; Manman Gao, Department of Orthopedics, Fuzhou Second Hospital, 350007 Fuzhou, Fujian, China. Email: gaomanm@mail2.sysu.edu.cn; Zhiyu Zhou, Department of Orthopaedic Surgery, Innovation Platform of Regeneration and Repair of Spinal Cord and Nerve Injury, The Seventh Affiliated Hospital, Sun Yat-sen University, 510275 Shenzhen, Guangdong, China; Guangdong Provincial Key Laboratory of Orthopedics and Traumatology, The First Affiliated Hospital of Sun Yat-sen University, 510060 Guangzhou, Guangdong, China. Email: zhouzhy23@mail.sysu.edu.cn

## Introduction

Physical activity is intricately linked to human health, with the potential to substantially reduce mortality rates, encompassing all-cause mortality (Kraus *et al*., 2019), cardiovascular disease, diabetes, and certain tumors (Bull *et al*., 2020; Moore *et al*., 2016; Rezende *et al*., 2018). As physical activity guidelines have evolved, the concept of vigorous intermittent lifestyle physical activity (VILPA) has gained prominence. VILPA encompasses brief, sporadic episodes of vigorous physical activity, lasting up to one or two minutes, as an integral part of daily life (Stamatakis *et al*., 2021; Stamatakis *et al*., 2019). Recent data have shown a growing body of evidence suggesting that VILPA could decrease the risk of all-cause mortality, coronary artery disease, and tumor-related mortality (Ahmadi *et al*., 2023; Stamatakis *et al*., 2022).

Physical activity contributes significantly to human health, involving numerous physiological pathways, with diverse and complex molecular mechanisms at the cellular level, in which $Ca^{2+}$ plays a pivotal role as a crucial second messenger in processes like muscle cell contraction, cell adhesion, cell cycle progression, cell growth, cell motility, and cell differentiation (McCarron *et al*., 2017). The irreplaceable role of $Ca^{2+}$ in sustaining normal physiological function is integral to the overall promotion of health.

The initial process involves mechanical stimuli acting on various organ tissues. It is suggested that cells may directly perceive short-time mechanical stimuli, but the mechanisms behind this perception are not yet fully understood. This process may require the conversion of mechanical signals into biological signals, exerting widespread effects on downstream pathways. The involvement of mechanosensors in this process has been sparsely documented. The molecular landscape governing mechanotransduction is diverse, and we explored into several common and widely impactful mechanosensitive molecules, namely *PIEZO1/2*, *TRPV4*, *KCNK2*, and *TMEM63A/B*. Our investigation revealed distinctive and regular alterations in *PIEZO1* expression following short-time stretching stimuli. PIEZO1, primarily expressed in non-excitable cellular domains, assumes a pivotal mantle in the transduction of mechanical stimuli, both intracellular and extracellular in origin, thereby orchestrating a multifaceted role across a spectrum of physiological and pathological milieus (Bagriantsev *et al*., 2014; Martins *et al*., 2016; Murthy *et al*., 2017; Ranade *et al*., 2014). PIEZO1 functions as a non-selective cation channel, primarily facilitating the influx of $Ca^{2+}$ (Lewis and Grandl, 2020; Wu *et al*., 2017; Zheng *et al*., 2019), which, in turn, participate as second messengers in the regulation of various downstream signaling pathways, profoundly influencing a spectrum of physiopathological processes. The activity of PIEZO1 is characterized by its transient and short-lived nature (Lewis *et al*., 2017; Nosyreva *et al*., 2021; Wijerathne *et al*., 2023; Yang *et al*., 2022; Zhao *et al*., 2018), coinciding with VILPA characteristics.

Building upon this foundation, this study delves into the dynamics of PIEZO1 response triggered by short-time stretch stimulation of hUCMSCs. It finds that cells primarily sense short-time mechanical stimuli through PIEZO1, predominantly mediated by regulated $Ca^{2+}$ influx. This is accompanied by delayed, oscillatory changes in PIEZO1 mRNA and protein levels. This underscores PIEZO1's crucial role in cellular responsiveness to transient mechanical cues, advancing our understanding of mechanosensory mechanisms in cellular physiology.

## Materials and Methods

### *Cell Isolation and Culture*

In this study, hUCMSCs were successfully isolated from umbilical cords following established protocols, identified (Zhang *et al*., 2021), and then subjected to experiments at P3–4.

The umbilical cords used in this study were approved by the Ethics Committee of the Seventh Affiliated Hospital of Sun Yat-sen University (Permit Number: 2019SYSUSH-031), and informed consent was obtained from the participants and their families. Briefly, the umbilical cord was washed 3 times with phosphate-buffered saline (PBS) containing 2 % v/v penicillin/streptomycin within 2 hours after *ex vivo* and removed umbilical vessels from Wharton's jelly. Then Wharton's jelly was cut into pieces about 1 $mm^3$ in size, evenly spread in the 6-well plate and placed upside down at 37 °C in a 5 % $CO_2$ humidified incubator for 30 min, and then added MSC special medium (Prim® hMSC SF-M, Premedical Laboratories Co., Ltd., Beijing, China) for culturing and changed the medium every 3 days. Digested when the confluence of the cells reaches about 80 %, subcultured at a density of 8000–10,000 cells per square centimeter ($cm^2$), and used Dulbecco's Modified Eagle Medium-Nutrient Mixture F-12 (Cat NO. C11330500BT, ThermoFish, Waltham, MA, USA) medium for culture.

### *Cell Stretch*

We employed a meticulously designed custom apparatus, which facilitates uniaxial cyclic stretching, offering adjustable parameters including frequency, amplitude, and duration. The stretching amplitude varies in a sinusoidal pattern over time while maintaining conditions akin to an incubator environment (5 % $CO_2$, 37 °C). A concise overview is provided herein, and please refer to the literature for details (Zhu *et al*., 2023).

Post-sterilization of the culture chamber, a coating of collagen I (Cat NO. A1048301, ThermoFish, Waltham, MA, USA) was applied, and cells were seeded at a density of $1 \times 10^4$ cells/$cm^2$. Following a 24–48 h incubation, cells achieved 60–70 % confluence, underwent a 12-hour period of nutrient deprivation, and were subsequently replenished with fresh complete medium. Ensuring pre-stretched readi-

ness, the pulley system was engaged. Stretching parameters were meticulously calibrated, and upon achieving stability, stretching stimulation was conducted, adhering to the pertinent parameters aligned with the experimental plan (stretching amplitude 10 %, stretching frequency 0.25/0.5/1.0 Hz, stretching time 0/0.5/1/2/4 minutes).

*Imaging of Intracellular $Ca^{2+}$ and Data Analysis*

HUCMSCs were cultured to 60–70 % confluence, followed by a triple wash with Hank's Balanced Salt Solution (HBSS). Pre-treatments were conducted using GsMTx4 (5 μM (Gnanasambandam *et al*., 2017), Cat NO. HY-P1410, ThermoFish, Waltham, MA, USA) according to the experimental design when required, following the instructions provided for the reagent. An appropriate concentration of Fluo-4 AM (Cat NO. F14201, ThermoFish, Waltham, MA, USA), supplemented with F-127 (Cat NO. P3000MP, ThermoFish, Waltham, MA, USA) at a concentration of 0.1 % (v/v), was prepared according to reagent guidelines and incubated for 30 minutes. Afterward, the liquid containing Fluo-4 AM was removed, and the cells were washed once with HBSS. Subsequently, the cells were incubated for an additional 10 minutes in HBSS.

The initial cell state was observed and captured using an inverted fluorescence microscope with a x10 objective lens. Subsequent experimental procedures, such as stretching or the addition of the PIEZO1 activator Yoda1 (Cat NO. SML1558-5MG, Merck & Co Inc, Shanghai, China), were carried out according to the predetermined plan. Immediate and sequential image capture was performed under consistent parameters, with a frame rate of 20 frames per minute for a duration of 3 to 5 minutes.

The images acquired were processed and analyzed using Image J software (version 1.54a, National Institutes of Health, Bethesda, MD, USA). Initially, the fluorescence values of images within the same group were quantified. Subsequently, the fluorescence values of images taken before treatment (such as stretching stimulation or Yoda1 activation) were used as a baseline ($F_0$) and images at different time points after treatment were normalized to this baseline ($F/F_0$). Finally, the relative increment changes in average fluorescence values at different time points were obtained to reflect the entry of $Ca^{2+}$ into the cytoplasm. Each sample was analyzed once, and each experimental group underwent at least three repetitions.

*Virus Packaging and Cell Transfection*

HEK293T cells were plated at a density of $1.0 \times 10^5$ cells/cm$^2$ and cultured in DMEM (Cat NO. C11995500BT, ThermoFish, Waltham, MA, USA) supplemented with 10 % FBS, while without penicillin-streptomycin. The day after plating, when the cells reached approximately 70 % confluence, the medium was changed to fresh medium without FBS. Subsequently, the hU6-MCS-CBh-gcGFP-IRES-puromycin (Table 1) plasmid (8.4 μg) was added. Then, 37.8 μL of Lipofectamine 3000 (Cat NO. L3000015, ThermoFish, Waltham, MA, USA) was used for co-transfection with the second-generation packaging plasmid (6.3 μg psPAX2, HedgehogBio Sci and Tec Ltd., Shanghai, China) and the envelope plasmid (4.2 μg pMD2.G, HedgehogBio Sci and Tec Ltd., Shanghai, China). After 6–8 hours of transfection, the medium was changed to complete medium, and lentiviruses were collected through conditioned medium 48 and 72 h post-transfection. The lentiviral supernatant was filtered through a 0.45 μm filter to remove residual cellular debris. MSCs were seeded in 100 mm dishes at a density of $1.0 \times 10^4$ cells/cm$^2$. The next day, samples were infected with 1000 μL of lentivirus containing shRNA fragments or vectors. Transfected cells were screened with 1.5 μg/mL puromycin. Cells were cultured in DMEM/F12 for 4 days and then collected for RNA and protein extraction for subsequent experiments.

*RNA Extraction, Reverse Transcription and RT-qPCR Analysis*

Total RNA extraction was conducted using the RNA Isolation Kit (Cat NO. R0027, Beyotime, Shanghai, China) in strict accordance with the manufacturer's protocols. The RNA isolation procedure comprised a temperature sequence of 37 °C for 15 minutes, followed by a 5-second exposure at 85 °C, and concluded with maintenance at 4 °C. Subsequently, 400 ng of RNA was subjected to reverse transcription alongside 4 μL of the provided mix (Cat NO. RR036A, Takara, Beijing, China), and the volume was adjusted to 20 μL with nuclease-free water. The resultant cDNA was further diluted fivefold with 1× TE buffer. Real-time quantitative PCR (RT-qPCR) analysis was performed using the PowerUp™ SYBR™ Green Master Mix (Cat NO. A25742, ThermoFisher, Waltham, MA, USA). A specific program was executed following established protocols (Zhu *et al*., 2023). Data analysis encompassed normalization against the GAPDH gene expression, employing the $2^{-\Delta\Delta Ct}$ algorithm. Customized and purified primers, designed using Primer 6.0 software, were synthesized (Sangon Biotech Co., Ltd., Shanghai, China). The primer sequences employed in this research are presented in Table 2.

*Protein Extraction and Treatment*

Proteins were extracted with RIPA buffer (Cat NO. 89900, ThermoFisher, Waltham, MA, USA) following the manufacturer's protocol. In brief, the culture medium was discarded, and the cells were washed twice with cold PBS. Cold RIPA buffer, cocktail inhibitors (Cat NO. 78430, ThermoFisher, Waltham, MA, USA), and phosphatase inhibitor (Cat NO. P1260-1ml, Solarbio, Beijing, China) were added to lyse the cells. The mixture was left to stand for 5 minutes, with occasional swirling to ensure even distribution. The lysate was collected using a pre-chilled scraper and transferred to microcentrifuge tubes. Centrifugation

**Table 1. Sequence of shRNA (hU6-MCS-CBh-gcGFP-IRES-puromycin).**

| ID | 5′ | stem | loop | stem | 3′ |
|---|---|---|---|---|---|
| **Sh1-a** | Ccgg | GCGTCTTCCTTAGCCATTACT | CTCGAG | AGTAATGGCTAAGGAAGACGC | TTTTTg |
| **Sh1-b** | aattcaaaaa | GCGTCTTCCTTAGCCATTACT | CTCGAG | AGTAATGGCTAAGGAAGACGC | |
| **Sh2-a** | Ccgg | GCTACGAGAACAAGCCCTACT | CTCGAG | AGTAGGGCTTGTTCTCGTAGC | TTTTTg |
| **Sh2-b** | aattcaaaaa | GCTACGAGAACAAGCCCTACT | CTCGAG | AGTAGGGCTTGTTCTCGTAGC | |
| **Sh3-a** | Ccgg | GCGTCATCATCGTGTGTAAGA | CTCGAG | TCTTACACACGATGATGACGC | TTTTTg |
| **Sh3-b** | aattcaaaaa | GCGTCATCATCGTGTGTAAGA | CTCGAG | TCTTACACACGATGATGACGC | |

**Table 2. Primers used for qRT-PCR in our research.**

| Gene | Primer (5′-3′) | Primer sequence |
|---|---|---|
| ***Piezo1*** | Forward | ATGTTGCTCTACACCCTGACC |
| | Reverse | CCAGCACACACATAGATCCAGT |
| ***Piezo2*** | Forward | CACGTTGGTGAGCCTTGAAG |
| | Reverse | TCAAACTCCGGGTTACTCTGT |
| ***KCNK2*** | Forward | TGGTGGTTGTCCTCTATCT |
| | Reverse | ATGGTGGTCCTCTGTGAA |
| ***TMEM63A*** | Forward | CACCACACTCAGTCCATTA |
| | Reverse | CTCCACAGTCTCCTTCCT |
| ***TMEM63B*** | Forward | CTCTTCTGGCTGCTCTTC |
| | Reverse | CTCCGTGTGCTCAATCTT |
| ***GAPDH*** | Forward | TGTGGGCATCAATGGATTTGG |
| | Reverse | ACACCATGTATTCCGGGTCAAT |

qRT-PCR, quantitative Real-time PCR.

was performed at 14,000 ×g for 15 minutes to collect the total protein, followed by transfer to new centrifuge tubes. The entire process was conducted on ice. The protein concentration was determined using the BCA protein assay kit (Cat. No. P0012, Beyotime, Shanghai, China), and the concentration was adjusted based on the results obtained. Finally, the protein was boiled for 10 minutes and reserved for the following experiment.

*Western Blot (WB)*

In accordance with the established laboratory procedures, proteins underwent electrophoresis utilizing Pre-Cast 4–12 % gradient Gels (Cat NO. NP0335BOX, ThermoFisher, Waltham, MA, USA) to achieve optimal separation. Subsequently, the proteins were transferred onto a PVDF membrane using the iBlot™ 2 Dry Blotting System (ThermoFisher, Waltham, MA, USA), following the precise guidelines provided by the manufacturer. The membrane was then subjected to blocking for one hour using 5 % non-fat powdered milk (Cat NO. D8340, Solarbio, Beijing, China) in 1× Tris Buffered Saline with Tween 20 (TBST). Following the blocking step, the membrane was incubated overnight at 4 °C with the specific primary antibody. Afterward, a suitable secondary antibody was applied, and the incubation continued for an additional hour at room temperature. To ensure proper antibody binding, the membrane was washed thrice for 10 minutes each time with 1xTBST. The protein expression was assessed using a gel imaging system in conjunction with an ECL chemiluminescence kit (Cat NO. SQ101, EpiZyme, Shanghai, China). Quantitative analysis of the bands was performed using Image J software to analyze the grayscale values. GAPDH was employed as an internal control throughout this research study. The details of all antibodies employed in this research are provided below: anti-PIEZO1 (Cat NO. MA5-32876, ThermoFisher, Waltham, MA, USA), anti-GAPDH (Cat NO. 2118S, Cell Signaling Technology, Danvers, MA, USA), second-antibody (Cat NO. A21010, ThermoFisher, Waltham, MA, USA).

*Statistical Analysis*

Quantitative data were obtained from a minimum of three replicative experimental iterations, and expressed as mean ± standard deviation (SD) or mean ± standard error of mean (SEM) in the resultant formation dataset. Statistical analyses employed SPSS version 20. Significance was assessed using an unpaired Student's *t*-test for two-group comparisons and a one-way ANOVA for three or more samples and multiple *t*-test with adjusted *p*-value by Bonferroni correction, with data conforming to standard distribution and aligned variance. Statistical significance was established at a threshold of $p < 0.05$ (ns not significant, * $p < 0.05$, ** $p < 0.01$, *** $p < 0.001$ and **** $p < 0.0001$).

## Results

*Yoda1 Stimulation: $Ca^{2+}$ Influx Initial Peak and PIEZO1 Activation Lasting One Minute*

The research involved the determination of optimal concentrations for two key components: the $Ca^{2+}$ fluorescent probe, Fluo-4 AM 1 μM, and the PIEZO1 activator, Yoda1 30 μM. The line chart suggests that the most significant changes in relative fluorescence intensities for Fluo-4 AM and Yoda1 occurred at concentrations of 1 μM and 30 μM, respectively (Fig. 1**A**). It is noteworthy that, unless explicitly specified otherwise, these optimal concentrations were consistently employed in all subsequent experiments.

In contrast to the control group, stimulation of human hUCMSCs with Yoda1 elicited an immediate surge in $Ca^{2+}$ influx, a phenomenon that persisted for approximately 60 seconds (Fig. 1**B,C**, $p < 0.05$). During this phase, a peak relative fluorescence was observed, surpassing baseline to 2× level, eventually converging to levels akin to the control group by the 90-second mark (Fig. 1**B,C**, **Supplementary Fig. 1A**). Upon transitioning to a $Ca^{2+}$-free D-Hanks extracellular medium, Yoda1 administration also appeared to induce an augmentation in $Ca^{2+}$ influx (Fig. 1**D**). However, when rigorously compared with the control group (**Supplementary Fig. 1B**), no statistically significant difference was discerned. In cases where pretreatment with the PIEZO1 inhibitor GsMTx4 was implemented, Yoda1 stimulation similarly resulted in increased $Ca^{2+}$ influx (Fig. 1**E,F**). Intriguingly, when the three experimental groups were subjected to a longitudinal comparative analysis in the absence of Yoda1 stimulation, the control group exhibited a noteworthy upsurge in $Ca^{2+}$ influx at the 120-second mark compared to the GsMTx4 group (Fig. 1**G,H**). Conversely, with Yoda1 stimulation, the control group displayed an even more pronounced and rapidly peaking increase in $Ca^{2+}$ influx within the initial 30 seconds (Fig. 1**I,J**). Notably, no significant distinctions were observed at other time points (**Supplementary Fig. 1E**). The time-dependent fluctuations in fluorescence intensity observed within the control and GsMTx4 groups provide indirect evidence of PIEZO1 activation and $Ca^{2+}$ influx. Representative fluorescence images of different groups at characteristic time points were shown in Fig. 1**K**.

*Optimal Stretching Stimulus Promotes PIEZO1 Activation and $Ca^{2+}$ Influx*

In this research, the dynamics of $Ca^{2+}$ influx resulting from the mechanical stimulation of hUCMSCs through uniaxial cyclic stretching. Various frequencies (0.25/0.5/1.0 Hz) and stretch durations (0.5/1/2/4 minutes) at a 10 % stretch amplitude were employed as experimental parameters. First and foremost, when the stretch stimulation was administered at a frequency of 0.25 Hz for varying durations (0.5/1/2/4 minutes), a notable observation emerged: $Ca^{2+}$ influx exhibited heightened levels across all stretch groups during the initial 30 seconds, gradually diminishing over time (Fig. 2**A**). Intriguingly, in some instances, $Ca^{2+}$ influx even dipped below the peak observed in the static control group by the 150-second mark (Fig. 2**D**, **Supplementary Fig. 2A**). Comparable outcomes were evident with 1.0 Hz stretch stimulation, reflecting a gradual decline in $Ca^{2+}$ influx across all stretch durations, albeit with a relatively extended period of elevated flow in the early phase (Fig. 2**C**). However, no significant deviation from the respective stretch groups was discerned at the peak when compared to the control group (**Supplementary Fig. 2B**). Subsequently, a resurgence in $Ca^{2+}$ influx was noted in the stretch group after 210 seconds (Fig. 2**G**).

The examination of $Ca^{2+}$ influx over a 5-minute period following stretch stimulation, at a frequency of 0.5 Hz, revealed consistent elevation in $Ca^{2+}$ levels within each stretch group in comparison to the control group. Additionally, each group exhibited distinct temporal trends (Fig. 2**B**). The fluorescence alterations at corresponding time points provided direct insights into the overall trajectory of each group's response (Fig. 2**F**). Notably, the 0.5-minute group displayed a gradual increase in $Ca^{2+}$ influx after 90 seconds, while the 4-minute group exhibited a slight and non-significant increase after 180 seconds (Fig. 2**B,F**). In contrast, the 1-minute group initially exhibited a higher $Ca^{2+}$ influx level after stimulation, which gradually diminished over the course of 5 minutes, eventually approaching the baseline state (Fig. 2**F**). While, the 2-minute group displayed a gradual increase in $Ca^{2+}$ influx beginning at the 40-second mark, reaching its zenith between 120 and 180 seconds (Fig. 2**B,F**, $p < 0.05$). During this peak period, $Ca^{2+}$ influx exceeded that of the other groups, with $F/F_0$ measurements reaching approximately 1.5 or higher. Subsequently, after the peak, $Ca^{2+}$ influx gradually declined (Fig. 2**F**, $p < 0.05$). Representative fluorescence images at specific time points after different duration of 0.5 Hz stretching were shown in Fig. 2**E**.

*Inhibitor GsMTx4 Decreases Stretch-induced PIEZO1 Activation and $Ca^{2+}$ Influx*

Within the GsMTx4 pretreatment group, the $Ca^{2+}$ influx exhibited distinct dynamics following stretch stimulation (0.5 Hz 2 minutes). Notably, the peak $Ca^{2+}$ influx manifested earlier in this group post-stretch and was distinctly higher than that observed in the control group within the initial 60 seconds. However, the amplitude of this peak was comparatively smaller, and no significant disparity was discerned when compared to the stretch group in relation to the control group (Fig. 3**A,B**). As time elapsed, the intracellular $Ca^{2+}$ influx within the GsMTx4 pretreatment group gradually declined, with no significant divergence from the control group and a significant reduction in comparison to the stretching group (Fig. 3**A,B**).

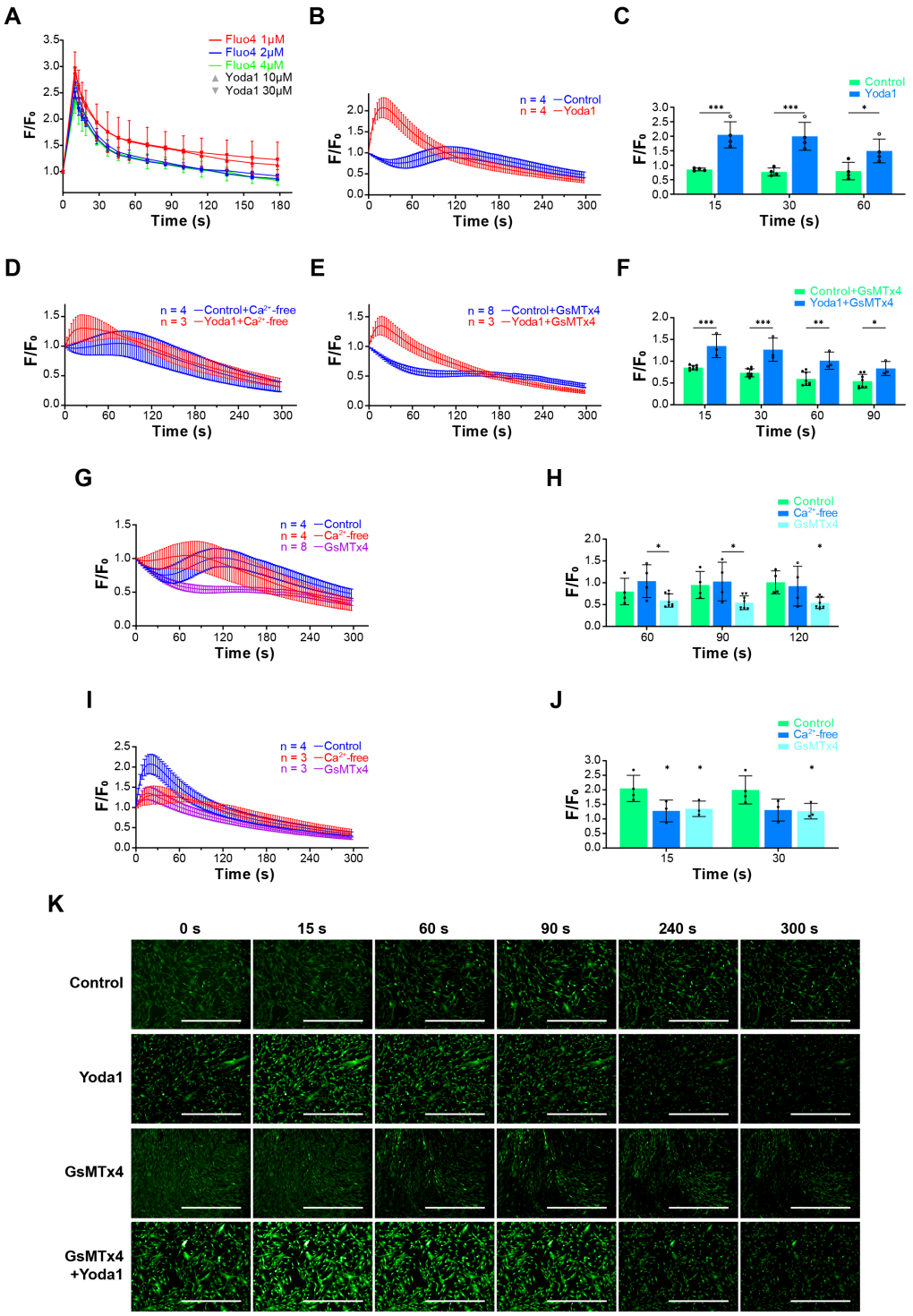


**Fig. 1. Activation of PIEZO1 and $Ca^{2+}$ influx for the first minute after Yoda1 stimulation.** (**A**) Changes in relative fluorescence intensity over time after incubation with 1/2/4 μM fluo4-AM and treatment with 10 μM and 30 μM Yoda1, respectively, with each group repeated independently three times. (**B,C**) Curves of changes in relative fluorescence intensity and statistical graphs of the differences between the control group at static and after treatment with Yoda1. (**D**) Curves of changes in relative fluorescence intensity of the $Ca^{2+}$-free group. (**E,F**) Curves of changes in relative fluorescence intensity and statistical graphs of the differences in the GsMTx4 pretreatment group. (**G,H**) Curves of changes in relative fluorescence intensity and statistical graphs of the differences among the three groups at static. (**I,J**) Curves of changes in relative fluorescence intensity and statistical graphs of the differences among the three groups after Yoda1 treatment. (**K**) representative fluorescent images of the control group and GsMTx4 pretreatment group at static and after Yoda1 treatment at different time. n, independent experiments, and the separate asterisks, relative to control group. Scale bars = 100 μm. All values were presented as mean ± SD. *: $p < 0.05$, **: $p < 0.01$; ***: $p < 0.001$.

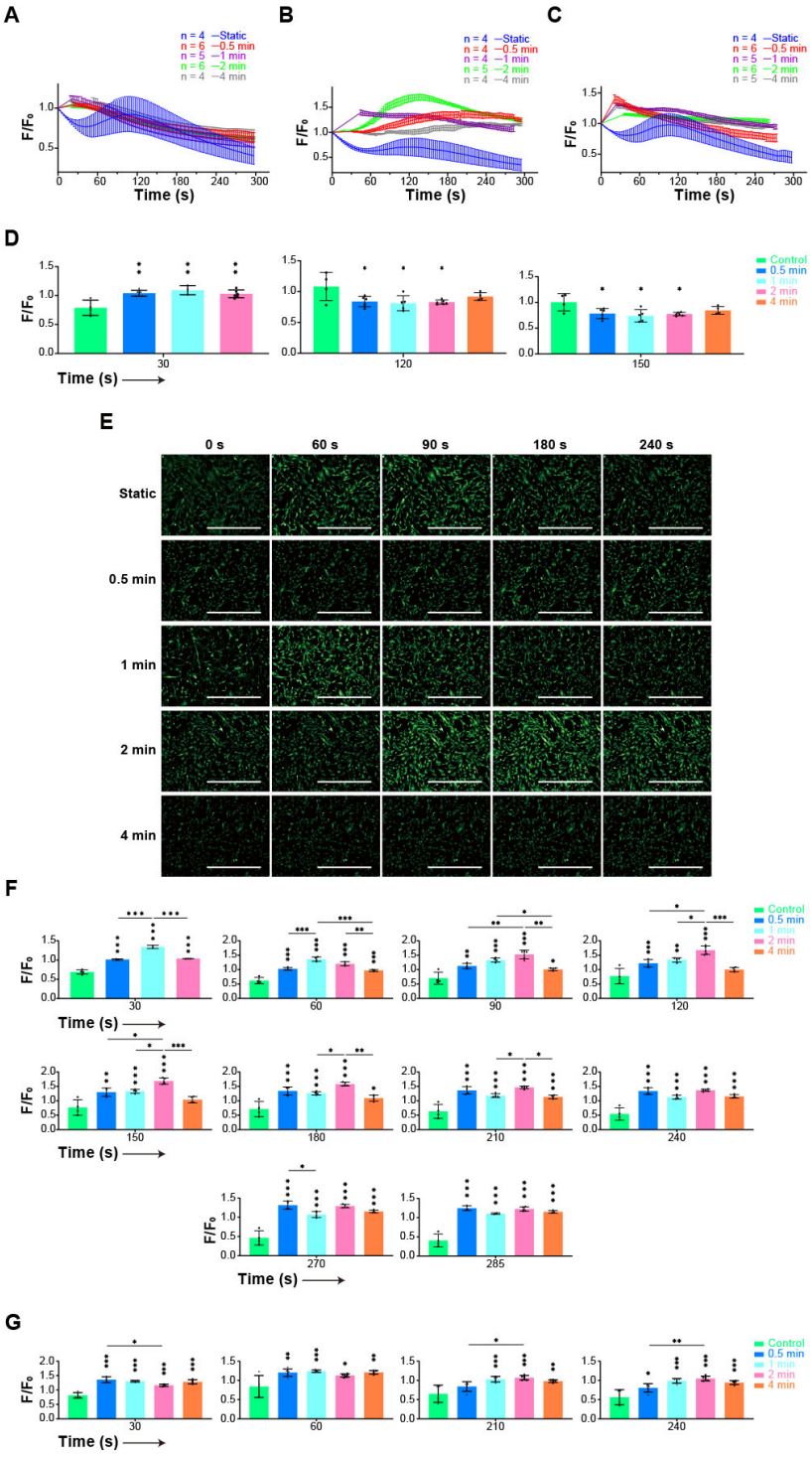


**Fig. 2. Changes in PIEZO1 activation and $Ca^{2+}$ influx regulated by different stretching stimuli.** (**A,D**) Changes in relative fluorescence intensity for 0.25 Hz stretching for 0, 0.5, 1, 2, and 4 minutes. Continuous change curves in (**A**) and statistical graphs of the changes in relative fluorescence intensity for each group at 30 s, 120 s and 150 s in (**D**). (**B,E,F**) Changes in relative fluorescence intensity for 0.5 Hz stretching for 0, 0.5, 1, 2, and 4 minutes. Continuous change curves in (**B**), representative fluorescent images of each group in (**E**), and relative fluorescence intensity for each group at 30 s, 60 s, 90 s, 120 s, 150 s, 180 s, 210 s, and 240 s in (**F**). (**C,G**) Changes in relative fluorescence intensity for 1.0 Hz stretching for 0, 0.5, 1, 2, and 4 minutes. Continuous change curve in (**C**) and the change in relative fluorescence intensity of each group at 30 s, 60 s, 210 s, and 240 s in statistical graphs. n, independent experiments, and the separate asterisks, relative to control group. Scale bars = 100 μm. All values were presented as mean ± SD. *: $p < 0.05$, **: $p < 0.01$; ***: $p < 0.001$.

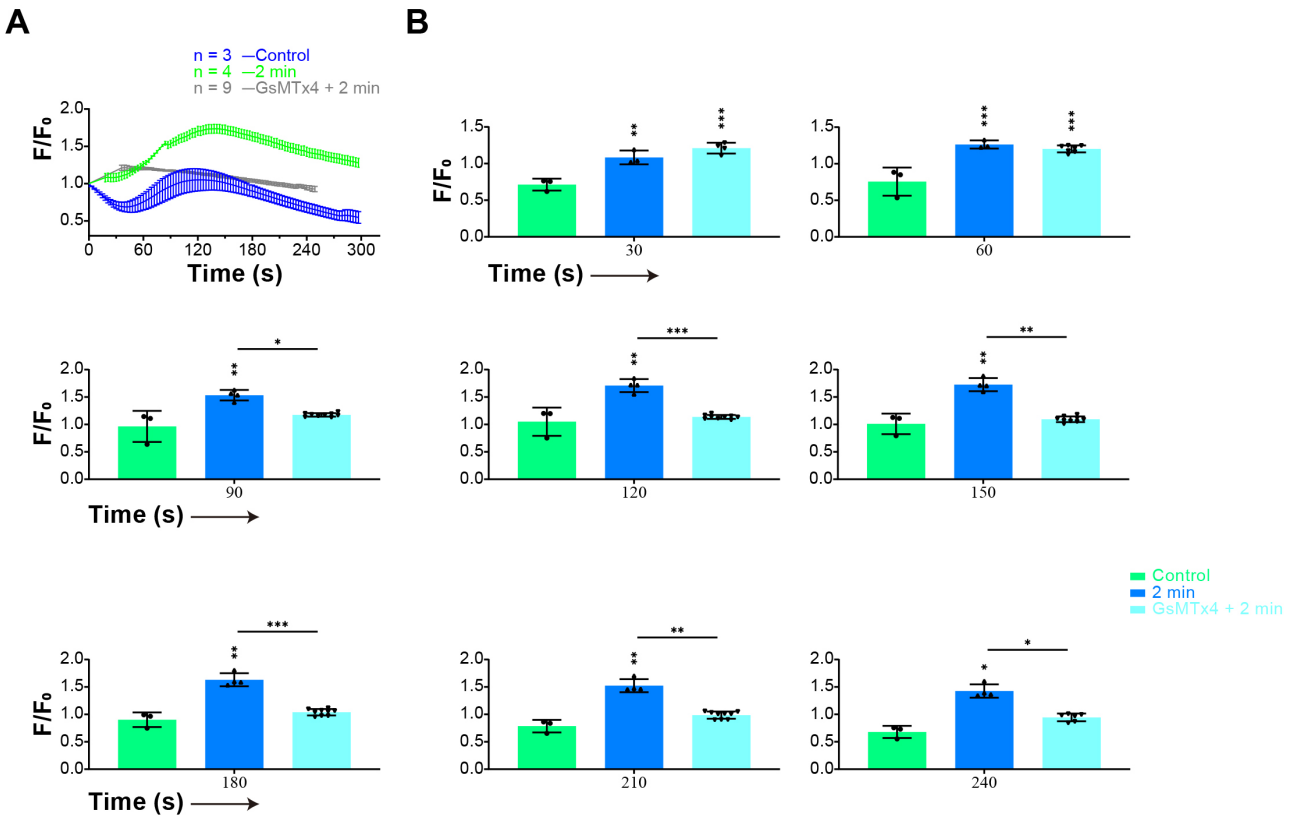


**Fig. 3. GsMTx4 decreases stretch-induced PIEZO1 activation and $Ca^{2+}$ influx.** (**A**) Changes in relative fluorescence intensity of the static group, the stretching (2 min, 0.5 Hz) group, and the stretching (2 min, 0.5 Hz) group after pretreatment with GsMTx4. (**B**) Relative fluorescence intensity of each group at 30 s, 60 s, 90 s, 120 s, 150 s, 180 s, 210 s, and 240 s, showing variations and differences. n, independent experiments, and the separate asterisks, relative to control group. All values were presented as mean ± SD. *: $p < 0.05$, **: $p < 0.01$; ***: $p < 0.001$.

*PIEZO1 Knockdown Diminishes $Ca^{2+}$ Influx Induced by Yoda1 and Stretching*

Initially, we engineered lentiviruses for *PIEZO1* knockdown and transfected them into hUCMSCs. Subsequently, we assessed the knockdown efficiency at the mRNA and protein levels, with the results indicating that the sh-1 and sh-3 achieved knockdown efficiencies of approximately 70 % (Fig. 4**A–C**). Subsequently, we selected the sh-3 group for further experimentation.

Under static conditions, the shPIEZO1 (*PIEZO1* knocked down) group $Ca^{2+}$ current exhibited a continuous decline, whereas the negative control (NC) or empty vector (EV) group displayed an increase at 60 seconds, eventually reaching levels akin to the initial state. This disparity was statistically significant when compared to the shPIEZO1 group (Fig. 4**D,E**). Furthermore, in the NC group, $Ca^{2+}$ influx began to decrease gradually at 120 seconds and remained similar to the shPIEZO1 group until 240 seconds (Fig. 4**D,E**, **Supplementary Fig. 3A**).

As Yoda1 stimulated, the early peak occurred slightly earlier in the shPIEZO1 group, with a significantly reduced amplitude, leading to an observable difference compared to the NC group (Fig. 4**F,G**). While the NC group experienced a sharp decline after the peak, no significant divergence was observed between the two groups. Toward the end of the observation period, $Ca^{2+}$ influx in the NC group was lower than that in the shPIEZO1 group (Fig. 4**F,G**, **Supplementary Fig. 3B**).

As stretch stimulation groups, the peak $Ca^{2+}$ influx in the shPIEZO1 group occurred significantly earlier, albeit with a lower amplitude and shorter duration. $Ca^{2+}$ influx was higher in the shPIEZO1 group only at the 30-second mark compared to the NC group (Fig. 4**H,I**, $p < 0.05$). Subsequently, $Ca^{2+}$ influx in the shPIEZO1 group continued to decrease, with no significant difference observed between the two groups at 60 seconds (Fig. 4**H**). However, $Ca^{2+}$ flux in the shPIEZO1 group was significantly lower than that in the NC group at all other time points (Fig. 4**I**). Representative fluorescence images of the NC and shPIEZO1 groups at various time points following a 2-minute, 0.5 Hz stretching protocol were shown in Fig. 4**J**.

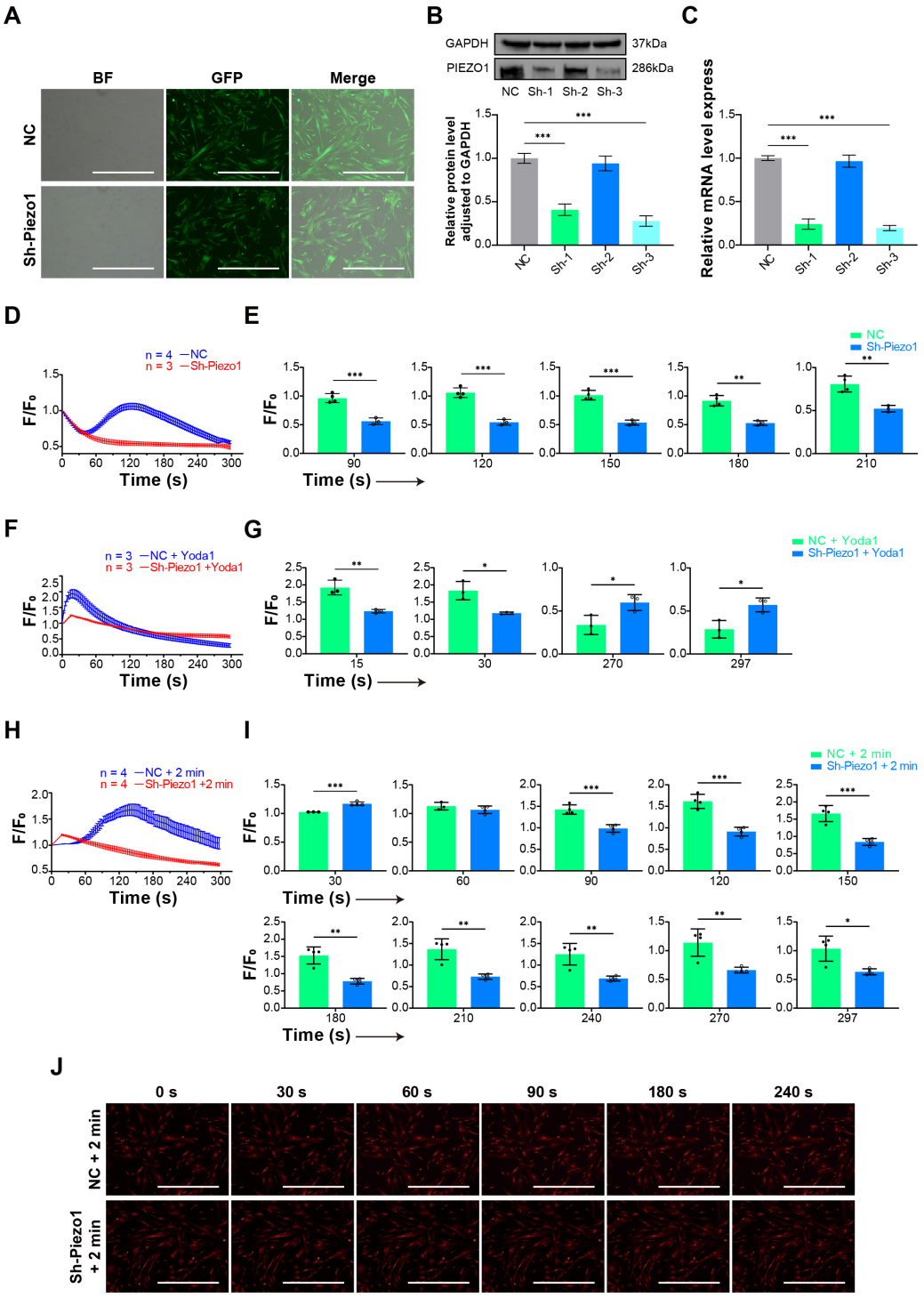


**Fig. 4. ShPIEZO1 reduces Yoda1 and stretch-induced PIEZO1 activity and $Ca^{2+}$ influx.** (**A–C**) *PIEZO1* was successfully knocked down. Cells were transfected with lentiviral vectors marked with green fluorescent protein (GFP) in (**A**). Western Blot (WB) results and statistics of gray values of the bands in the NC group and shPEIZO1 group in (**B**). mRNA expression in (**C**). n = 3. (**D,E**) Changes in relative fluorescence intensity at static conditions, with a continuous change curve in (**D**), and statistics graphs of relative fluorescence intensity in (**E**). (**F,G**) Changes in relative fluorescence intensity after Yoda1 stimulation, with a continuous change curve in (**F**), and statistics graphs of relative fluorescence intensity in (**G**). (**H–J**) Relative fluorescence intensity changes after stretching for 2 minutes, with a continuous change curve in (**H**) and statistics graphs of relative fluorescence intensity in (**I**), and representative fluorescent images of each group in (**J**). NC, negative control (or vector). n, independent experiments. Scale bars = 100 μm. Values, in B and C, were presented as mean ± SEM, and others as mean ± SD. *: $p < 0.05$, **: $p < 0.01$; ***: $p < 0.001$.

*PIEZO1 mRNA and Protein Dynamics in Response to Varied Stretching Time and Interval*

Beyond the evident influence of stretch stimulation on PIEZO1 activation and the consequential alterations in $Ca^{2+}$ influx, we aimed to determine whether this mechanosensitive process was accompanied by corresponding shifts in gene and protein levels. To explore this, we subjected samples to 0.5 Hz (10 %) stretch stimulation for varying durations (2/5/10/15 minutes) and meticulously extracted total RNA at distinct time intervals (0/15/30/60 minutes). Our rigorous examination aimed to unveil fluctuations in *PIEZO1* mRNA expresses, as well as potential shifts in mRNA levels pertaining to commonly observed mechanosensitive markers. The outcomes revealed a distinct pattern in *PIEZO1* mRNA expression, characterized by dual peaks manifesting within the initial hour following stretch stimulation at various durations (Fig. 5**A**). Remarkably, the first of these peaks, occurring 15 minutes post-stretching, exhibited greater prominence, particularly evident in the 10-minute group (Fig. 5**A**, $p < 0.05$). However, it is worth noting that no clear, consistent pattern of change was observed across diverse stretch durations at each time point (Fig. 5**B**).

Diverse durations (5/10/15 minutes) of stretching stimuli led to a general reduction in Piezo2 mRNA levels (**Supplementary Fig. 4A**). Notably, Piezo2 mRNA exhibited relatively higher levels when subjected to 2 minutes of stretching stimulation at different time points (**Supplementary Fig. 4B**). Conversely, other commonly mechanosensitive molecules, including TRPV4 KCNK2 and TEME6A/B, displayed either no significant alterations or exhibited changes lacking a discernible pattern (**Supplementary Fig. 4C,D**). The findings from the aforementioned investigations have illuminated that a brief 10-minute bout of stretching at specific intervals can indeed elicit alterations in *PIEZO1* mRNA expression. To comprehensively assess the corresponding modifications in protein levels, we established a temporal framework encompassing five distinct time points (0/0.5/1/2/4 hours). The results obtained through western blot analysis unveiled a discernible trend in PIEZO1 protein dynamics. Notably, an initial upsurge in PIEZO1 protein levels commenced at1 hour post-stretching and had essentially reached its zenith by the 2-hour mark (Fig. 5**C,D**, $p < 0.05$).

## Discussion

VILPA could decrease the risk of related diseases and confer health benefits (Ahmadi *et al*., 2023; Stamatakis *et al*., 2022), and in this study, cells discern short-time mechanical stimuli via the PIEZO1 protein. Our investigation shows that during resting state, PIEZO1 functionality maintains a state of low-level dynamic equilibrium. Upon exposure to brief mechanical stimuli, a notable dynamic shift occurs in PIEZO1's functional state. The inhibitor GsMTx4 effectively attenuated the fluctuations but did not entirely suppress the Yoda1-induced calcium influx. GsMTx4 interacts independently of peptides and channels at membrane or membrane-protein interfaces and primarily reduces the mechanosensitivity of PIEZO1 by modulating membrane tension (Bae *et al*., 2011; Gnanasambandam *et al*., 2017; Suchyna *et al.*, 2004). In contrast, Yoda1 predominantly stabilizes PIEZO1, thereby slowing down its inactivation phase (Syeda *et al*., 2015). Additionally, a knockdown of PIEZO1 expression substantially mitigates functional oscillation. Ongoing inquiries into PIEZO1 underscore its heightened mechanosensitivity, prompt functional alterations, and a subsequent refractory period post-activation (Lewis and Grandl, 2015; Wijerathne *et al*., 2022; Yang *et al*., 2022), aligning seamlessly with established findings.

However, in the process of responding to short-time mechanical stimuli via PIEZO1, it elicits a transient $Ca^{2+}$ influx. $Ca^{2+}$, serving as a second messenger, transmits diverse signals at the cellular level and impacts a broad spectrum of physiological functions. For instance, $Ca^{2+}$ participates in regulating signaling pathways such as Notch (Wang *et al*., 2020; Wang *et al*., 2021), TGF-$\beta$ (Jairaman *et al*., 2021), NFAT (Zhou *et al*., 2020), RhoA (Inaba *et al*., 2021; Tsuchiya *et al.*, 2018), and Wnt (Wong *et al*., 2018), which govern cellular functions including proliferation, differentiation, migration, and metabolism. Consequently, these processes influence the physiological or pathological processes of the organism. In summary, transient cellular-level stimulation orchestrates the influx of $Ca^{2+}$ through PIEZO1, eliciting a spectrum of effects.

While alternative mechanoreceptor and transducer molecules may contribute to brief mechanical stimuli, their primary role remains secondary. PIEZO2 is predominantly found in sensory neurons and the respiratory tract. Previous research has shown that PIEZO2 exhibits high sensitivity to cell membrane indentation (Ikeda and Gu, 2014; Moroni *et al*., 2018; Shin *et al.*, 2019), but its sensitivity to stretching is relatively low (Coste *et al.*, 2015; Moroni *et al*., 2018; Verkest *et al*., 2022). Our findings in hUCMSCs also indicate that PIEZO2's response to stretching is less pronounced compared to PIEZO1. The regulation of the transient receptor potential (TRP) superfamily remains debated. Some studies suggest TRP channels aren't sensitive to cell membrane stretching (Nikolaev *et al*., 2019) but may be activated by cytoplasmic tethers (Yang *et al*., 2018). In contrast, TRPV4 responds to cell-substrate contact, unlike PIEZO1 activated by membrane stretching (Servin-Vences *et al*., 2017). The role of cytoskeletal stretching in TRP channel activation, however, remains unclear. In this investigation, TRPV4 displayed only marginal upregulation at the mRNA level without marked oscillations. Conversely, adhesion proteins and integrins predominantly perceive external mechanical stimuli through interactions with the extracellular matrix (Campbell and Humphries, 2011; Li *et al*., 2016; Valdivia *et al*., 2023). This intricate process involves the engagement of a larger array of protein

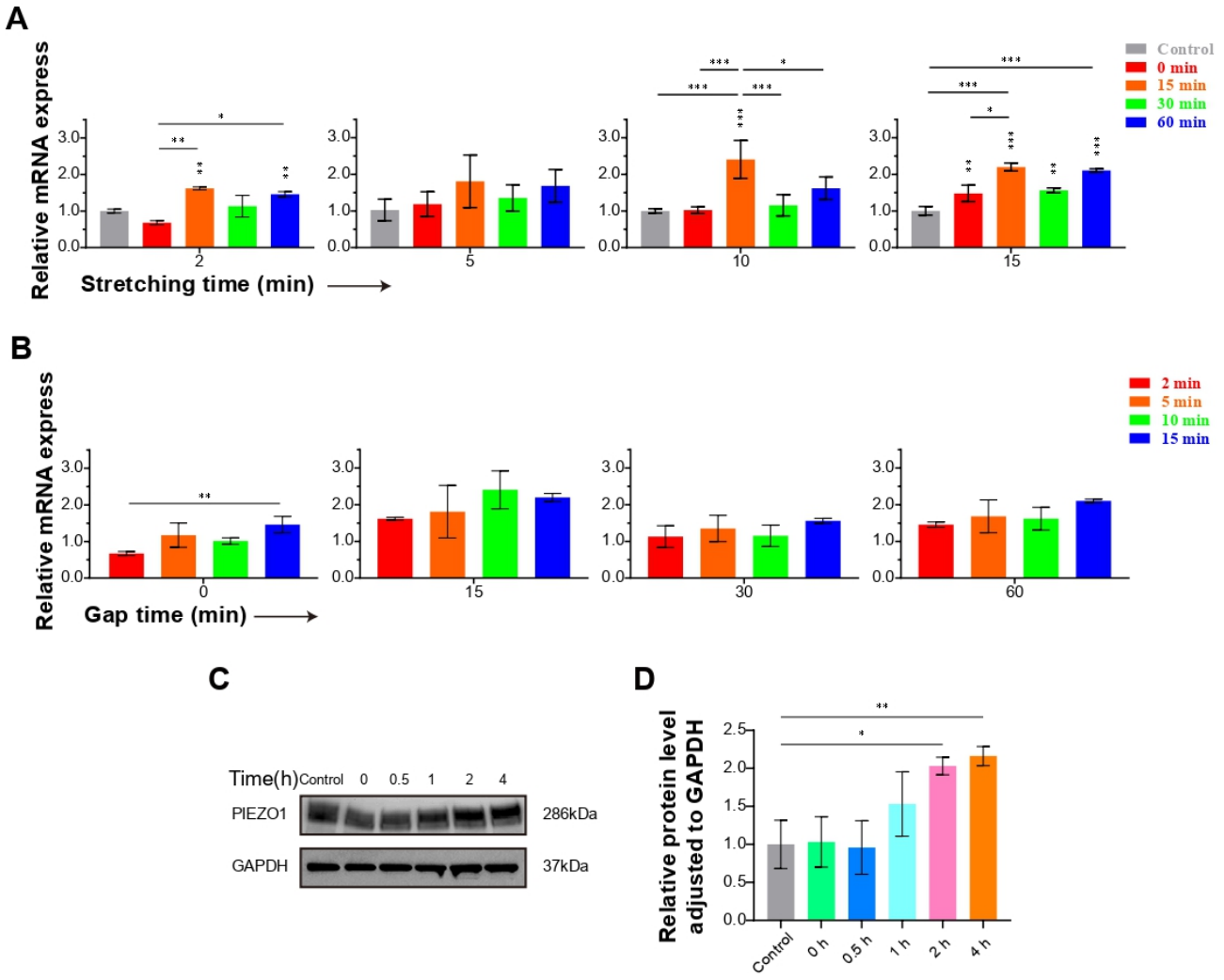


**Fig. 5. *PIEZO1* mRNA and protein delayed elevation induced by short-term stretching stimulus.** (**A**) Results of qPCR for *PIEZO*1 after 0.5 Hz 10 % continuous stretching for 2, 5, and 10 minutes. Results for different time points with the same stretching duration are shown in (**A**) and results at the same time points with different duration stretching stimuli are presented in (**B**). (**C**) WB results showing PIEZO1 changes before and at 0, 0.5, 1, 2, and 4 hours after 0.5 Hz 10 % stretching for 10 minutes. (**D**) Statistics for the grey value analysis of WB bands in C. n = 3, and the separate asterisks, relative to control group. All values were presented as mean ± SEM. *: $p < 0.05$, **: $p < 0.01$; ***: $p < 0.001$.

molecules and exerts a more pronounced influence on prolonged mechanical stimuli.

However, with the escalating duration of stretching, the temporal activation of PIEZO1 and the consequent substantial $Ca^{2+}$ influx manifest a non-linear correlation. Analogously, a akin pattern is discernible in the delayed oscillations of mRNA levels. The macroscopic ramifications of PIEZO1 channel opening predominantly derive from the stochastic activation of individual PIEZO1 molecules. The extension of stretching time does not propel each PIEZO1 molecule towards its activation threshold, as variables like the resurgence of PIEZO1 also factor into the equation (Lewis *et al*., 2017; Nosyreva *et al*., 2021; Wijerathne *et al*., 2023).

In studies involving uniaxial cyclic stretch-mechanical stimulation of cells, our findings indicate that appropriate stretch stimulation (0.5 Hz, 10 % for 2 minutes) can activate PIEZO1, resulting in a peak in channel opening between 90 to 180 seconds, subsequently leading to $Ca^{2+}$ influx. As previously mentioned, existing research predominantly suggests that PIEZO1 detects changes in membrane tension by perceiving alterations in local membrane curvature, consequently regulating various functional states (Haselwandter *et al*., 2022; Jiang *et al*., 2021; Yang *et al*., 2022). Within a defined range, elevating membrane tension enhances the likelihood of channel opening through accelerating the rate of channel opening and decelerating the closing process, meanwhile by lengthening the opening interval and shortening the

closing interval (Wijerathne *et al*., 2023). It is noteworthy that stretch-induced stimulation exhibits notable variations among individual cells due to several factors. hUCMSCs, characterized by short shuttle-shaped morphology, exhibit disordered polarity and orientation on the substrate, resulting in distinct stimulation profiles. Furthermore, variations in PIEZO1 protein distribution on hUCMSCs may also contribute to differences in cellular response. Regions near the end, where membrane tension is most pronounced, exhibit relatively higher sensitivity of PIEZO1 activation. These findings further substantiate the notion that alterations in waveforms resulting from mechanical stretch stimuli primarily stem from changes in PIEZO1 function.

Furthermore, a precise correlation between the amplitude of stretching and activity intensity has not been definitively established. Prior investigations into stretch stimulation primarily employed amplitudes within the range of 5–15 %, with no observed significant cellular damage yet (Cao *et al*., 2018; Chen and Wu, 2019; Mathieu *et al*., 2020; Yang *et al*., 2021). We selected stretching magnitude (10 %) in this investigation emulates a level approaching the upper threshold of cellular endurance.

In relation to PIEZO1 function, it is crucial to consider its dependence on the frequency of mechanical stimulation. Prior research has proposed a correlation between PIEZO1 opening and sinusoidal frequency, suggesting an augmented probability of PIEZO1 activation with increasing stimulus frequency within a specific range (Lewis *et al*., 2017). However, the scope of this study primarily encompasses a limited range of low-frequency variations, along with post-stimulus superimposed effects, which may yield distinct impacts on PIEZO1. The question arises as to whether the reduction in $Ca^{2+}$ influx represents an adaptive response orchestrated by PIEZO1 to accommodate novel mechanical stimuli (Lewis *et al*., 2017). Existing data indicate that adaptation plays a relatively minor role in $Ca^{2+}$ influx attenuation, with inactivation emerging as the predominant mechanism. Consequently, our study does not delve into this issue. Within our study, we subjected cells to stretch stimulation at a frequency of 0.25 Hz, revealing no significant disparities among groups. Notably, an initial decline in peak PIEZO1 opening was observed across all durations, with the middle period even exhibiting levels lower than the static control group. Contrastingly, at a frequency of 0.5 Hz, distinct variations emerged among groups during different time intervals. Specifically, for 0.5-minute and 4-minute stretches, PIEZO1 opening exhibited a gradual increase post-stretch, whereas a pronounced early peak followed by gradual decline was noted for the 1-minute stretch. Interestingly, the 2-minute stretch displayed a peak in the middle of the session. In Markov modeling, simulated studies have posited the existence of diverse states of PIEZO1 opening and closing, characterized by varying durations of open and closed states (Lewis *et al*., 2017; Nosyreva *et al*., 2021; Wijerathne *et al*., 2023). Lower frequencies, such as 0.25 Hz, may activate only a fraction of PIEZO1, leading to gradual inactivation toward the end of stretching. Conversely, elevated frequencies are closely associated with distinct states of opening and closing, hinting at a time-dependent stimulation influence on longer opening. The precise underlying mechanism is a focal point of our ongoing research efforts.

While our study explores PIEZO1's role in cellular $Ca^{2+}$ regulation in response to mechanical stimuli, we are keen to understand its relevance in living organisms. Given the challenges associated with direct animal modeling, we intend to utilize dynamic culture systems to develop *in vitro* organoid models. This approach will enable us to investigate cellular responses to short-term mechanical cues at a tissue level, identify key molecular pathways, and lay the groundwork for understanding the health implications of VILPA.

This study presents the following limitations. Firstly, it focused solely on a single cell type for validation and lacked validation at the tissue level or in vivo, which will be the focus of our next experimental steps. Additionally, there is attenuation in the fluorescence changes of Fluo4 AM, and the accuracy of $Ca^{2+}$ influx in the later stage is slightly lower than in the early stage. This limitation cannot be avoided or overcome in the experiment.

## Conclusions

In conclusion, our data evidenced that cells primarily sense short-time mechanical stimuli through PIEOZ1, predominantly mediated by regulated $Ca^{2+}$ influx. This underscores PIEZO1's crucial role in cellular responsiveness to transient mechanical cues, advancing our understanding of mechanosensory mechanisms in cellular physiology.

## List of Abbreviations

VILPA, vigorous intermittent lifestyle physical activity; hUCMSCs, human umbilical cord-derived mesenchymal stem cells; shRNA, short hairpin RNA; qRT-PCR, quantitative real-time polymerase chain reaction; WB, western blot; PBS, phosphate-buffered saline; HBSS, Hank's Balanced Salt Solution; TBST, Tris Buffered Saline with Tween 20; SD, standard deviation; SEM, standard error of mean; NC, negative control; EV, empty vector; GFP, green fluorescent protein; TRP, transient receptor potential.

## Declaration of AI and AI-assisted Technologies in the Writing Process

During the preparation of this work the authors used ChatGpt-3.5 in order to check spell and grammar. After using this tool, the authors reviewed and edited the content as needed and takes full responsibility for the content of the publication.

## Availability of Data and Materials

The data supporting the conclusions of this study are available from the corresponding author, Z.Y. Zhou, in addition to those included in the published manuscript.

## Author Contributions

FAW: administrative support, collection and assembly of data, data analysis and interpretation and manuscript writing. HKC: administrative support, collection and assembly of data and revise manuscript. ZYH: administrative support, collection and assembly of data and revise manuscript. JFL: collection and assembly of data and revise manuscript. ZYZhu: provision of study material and collection data. TT: provision of study material and collection data. JHL: provision of study material and collection data. JXZ: provision of study material and collection data. QXT: provision of study material and collection data. ZL: revise manuscript and assembly of data. MJS: revise manuscript and assembly of data. XZL: financial support, assembly of data and revise manuscript. MMG: Conception and design, assembly of data and revise manuscript. ZYZhou: Conception and design, financial support, final approval of the manuscript. SYL: financial support and final approval of manuscript. All authors contributed to editorial changes in the manuscript, read and approved the final manuscript, and have participated sufficiently in the work to take public responsibility for appropriate portions of the content. All authors have agreed to be accountable for all aspects of the work.

## Ethics Approval and Consent to Participate

This study was approved by the Ethics Committee at the Seventh Affiliated Hospital of Sun Yat-sen University, Shenzhen, China (NO. 2019SYSUSH-031), and informed consent was obtained from the participants and their families.

## Acknowledgments

Special thanks are extended to Gao Xiangshang from the Seventh Affiliated Hospital (Sun Yat-sen University, Shenzhen), Cheng Ruijuan from Active Technology Limited and Zhang Guangxu in Accuramed Technology (Shanghai) Limited (https://www.accuramed.com/) and FigDraw platform for support and help.

## Funding

Our research was supported by the National Natural Science Foundation of China (U22A20162, 31900583, 32071351, 81772400, 82102604, 81960395), foundation of Shenzhen Committee for Science and Technology Innovation (JCYJ20220530150417038), Sanming Project of Medicine in Shenzhen (SZSM201911002), the Beijing Municipal Health Commission (Grant No. BMHC-2021-6, BMHC-2019-9, BMHC-2018-4, PXM2020_026275_000002), Key Clinical Specialty Discipline Construction Program of Fuzhou, Fujian, P.R.C (20220104), AO CMF CPP on Bone Regeneration (AOCMF-21-04S, supported by AO Foundation, AO CMF. AO CMF is a clinical division of the AO Foundation - an independent medically-guided not-for-profit organization), Sun Yat-sen University Clinical Research 5010 Program (2019009), Academic Affairs Office of Sun Yat-sen University (20242043, 20242118, 20242144, 20242162).

## Conflict of Interest

The authors declare no conflict of interest. MJS is serving the Editorial Board members of this journal. We declare that MJS had no involvement in the peer review of this article and has no access to information regarding its peer review. Full responsibility for the editorial process for this article was delegated to CE.

## Supplementary Material

Supplementary material associated with this article can be found, in the online version, at https://doi.org/10.22203/eCM.v048a01.

## References

Ahmadi MN, Hamer M, Gill JMR, Murphy M, Sanders JP, Doherty A, Stamatakis E (2023) Brief bouts of device-measured intermittent lifestyle physical activity and its association with major adverse cardiovascular events and mortality in people who do not exercise: a prospective cohort study. The Lancet. Public Health 8: e800-e810. DOI: 10.1016/S2468-2667(23)00183-4.

Bae C, Sachs F, Gottlieb PA (2011) The mechanosensitive ion channel Piezo1 is inhibited by the peptide GsMTx4. Biochemistry 50: 6295-6300. DOI: 10.1021/bi200770q.

Bagriantsev SN, Gracheva EO, Gallagher PG (2014) Piezo proteins: regulators of mechanosensation and other cellular processes. The Journal of Biological Chemistry 289: 31673-31681. DOI: 10.1074/jbc.R114.612697.

Bull FC, Al-Ansari SS, Biddle S, Borodulin K, Buman MP, Cardon G, Carty C, Chaput JP, Chastin S, Chou R, Dempsey PC, DiPietro L, Ekelund U, Firth J, Friedenreich CM, Garcia L, Gichu M, Jago R, Katzmarzyk PT, Lambert E, Leitzmann M, Milton K, Ortega FB, Ranasinghe C, Stamatakis E, Tiedemann A, Troiano RP, van der Ploeg HP, Wari V, Willumsen JF (2020) World Health Organization 2020 guidelines on physical activity and sedentary behaviour. British Journal of Sports Medicine 54: 1451-1462. DOI: 10.1136/bjsports-2020-102955.

Campbell ID, Humphries MJ (2011) Integrin structure, activation, and interactions. Cold Spring Harbor Perspectives in Biology 3: a004994. DOI: 10.1101/cshperspect.a004994.

Cao C, Li L, Li H, He X, Wu G, Yu X (2018) Cyclic biaxial tensile strain promotes bone marrow-derived mesenchymal stem cells to differentiate into cardiomyocyte-like cells by miRNA-27a. The International Journal of Biochemistry & Cell Biology 99: 125-132. DOI: 10.1016/j.biocel.2018.04.004.

Chen J, Wu X (2019) Cyclic tensile strain promotes chondrogenesis of bone marrow-derived mesenchymal stem cells by increasing miR-365 expression. Life Sciences 232: 116625. DOI: 10.1016/j.lfs.2019.116625.

Coste B, Murthy SE, Mathur J, Schmidt M, Mechioukhi Y, Delmas P, Patapoutian A (2015) Piezo1 ion channel pore properties are dictated by C-terminal region. Nature Communications 6: 7223. DOI: 10.1038/ncomms8223.

Gnanasambandam R, Ghatak C, Yasmann A, Nishizawa K, Sachs F, Ladokhin AS, Sukharev SI, Suchyna TM (2017) GsMTx4: Mechanism of Inhibiting Mechanosensitive Ion Channels. Biophysical Journal 112: 31-45. DOI: 10.1016/j.bpj.2016.11.013.

Haselwandter CA, Guo YR, Fu Z, MacKinnon R (2022) Elastic properties and shape of the Piezo dome underlying its mechanosensory function. Proceedings of the National Academy of Sciences of the United States of America 119: e2208034119. DOI: 10.1073/pnas.2208034119.

Ikeda R, Gu JG (2014) Piezo2 channel conductance and localization domains in Merkel cells of rat whisker hair follicles. Neuroscience Letters 583: 210-215. DOI: 10.1016/j.neulet.2014.05.055.

Inaba H, Miao Q, Nakata T (2021) Optogenetic control of small GTPases reveals RhoA mediates intracellular calcium signaling. The Journal of Biological Chemistry 296: 100290. DOI: 10.1016/j.jbc.2021.100290.

Jairaman A, Othy S, Dynes JL, Yeromin AV, Zavala A, Greenberg ML, Nourse JL, Holt JR, Cahalan SM, Marangoni F, Parker I, Pathak MM, Cahalan MD (2021) Piezo1 channels restrain regulatory T cells but are dispensable for effector CD4+ T cell responses. Science Advances 7: eabg5859. DOI: 10.1126/sciadv.abg5859.

Jiang W, Del Rosario JS, Botello-Smith W, Zhao S, Lin YC, Zhang H, Lacroix J, Rohacs T, Luo YL (2021) Crowding-induced opening of the mechanosensitive Piezo1 channel in silico. Communications Biology 4: 84. DOI: 10.1038/s42003-020-01600-1.

Kraus WE, Powell KE, Haskell WL, Janz KF, Campbell WW, Jakicic JM, Troiano RP, Sprow K, Torres A, Piercy KL, 2018 PHYSICAL ACTIVITY GUIDELINES ADVISORY COMMITTEE* (2019) Physical Activity, All-Cause and Cardiovascular Mortality, and Cardiovascular Disease. Medicine and Science in Sports and Exercise 51: 1270-1281. DOI: 10.1249/MSS.0000000000001939.

Lewis AH, Cui AF, McDonald MF, Grandl J (2017) Transduction of Repetitive Mechanical Stimuli by Piezo1 and Piezo2 Ion Channels. Cell Reports 19: 2572-2585. DOI: 10.1016/j.celrep.2017.05.079.

Lewis AH, Grandl J (2015) Mechanical sensitivity of Piezo1 ion channels can be tuned by cellular membrane tension. eLife 4: e12088. DOI: 10.7554/eLife.12088.

Lewis AH, Grandl J (2020) Inactivation Kinetics and Mechanical Gating of Piezo1 Ion Channels Depend on Subdomains within the Cap. Cell Reports 30: 870-880.e2. DOI: 10.1016/j.celrep.2019.12.040.

Li Z, Lee H, Zhu C (2016) Molecular mechanisms of mechanotransduction in integrin-mediated cell-matrix adhesion. Experimental Cell Research 349: 85-94. DOI: 10.1016/j.yexcr.2016.10.001.

Martins JR, Penton D, Peyronnet R, Arhatte M, Moro C, Picard N, Kurt B, Patel A, Honoré E, Demolombe S (2016) Piezo1-dependent regulation of urinary osmolarity. Pflugers Archiv: European Journal of Physiology 468: 1197-1206. DOI: 10.1007/s00424-016-1811-z.

Mathieu PS, Fitzpatrick E, Di Luca M, Cahill PA, Lally C (2020) Resident multipotent vascular stem cells exhibit amplitude dependent strain avoidance similar to that of vascular smooth muscle cells. Biochemical and Biophysical Research Communications 521: 762-768. DOI: 10.1016/j.bbrc.2019.10.185.

McCarron JG, Lee MD, Wilson C (2017) The Endothelium Solves Problems That Endothelial Cells Do Not Know Exist. Trends in Pharmacological Sciences 38: 322-338. DOI: 10.1016/j.tips.2017.01.008.

Moore SC, Lee IM, Weiderpass E, Campbell PT, Sampson JN, Kitahara CM, Keadle SK, Arem H, Berrington de Gonzalez A, Hartge P, Adami HO, Blair CK, Borch KB, Boyd E, Check DP, Fournier A, Freedman ND, Gunter M, Johannson M, Khaw KT, Linet MS, Orsini N, Park Y, Riboli E, Robien K, Schairer C, Sesso H, Spriggs M, Van Dusen R, Wolk A, *et al*. (2016) Association of Leisure-Time Physical Activity With Risk of 26 Types of Cancer in 1.44 Million Adults. JAMA Internal Medicine 176: 816-825. DOI: 10.1001/jamainternmed.2016.1548.

Moroni M, Servin-Vences MR, Fleischer R, Sánchez-Carranza O, Lewin GR (2018) Voltage gating of mechanosensitive PIEZO channels. Nature Communications 9: 1096. DOI: 10.1038/s41467-018-03502-7.

Murthy SE, Dubin AE, Patapoutian A (2017) Piezos thrive under pressure: mechanically activated ion channels in health and disease. Nature Reviews. Molecular Cell Biology 18: 771-783. DOI: 10.1038/nrm.2017.92.

Nikolaev YA, Cox CD, Ridone P, Rohde PR, Cordero-Morales JF, Vásquez V, Laver DR, Martinac B (2019) Mammalian TRP ion channels are insensitive to membrane stretch. Journal of Cell Science 132: jcs238360. DOI: 10.1242/jcs.238360.

Nosyreva ED, Thompson D, Syeda R (2021) Identification and functional characterization of the Piezo1 channel pore domain. The Journal of Biological Chemistry 296: 100225. DOI: 10.1074/jbc.RA120.015905.

Ranade SS, Qiu Z, Woo SH, Hur SS, Murthy SE, Ca-

halan SM, Xu J, Mathur J, Bandell M, Coste B, Li YSJ, Chien S, Patapoutian A (2014) Piezo1, a mechanically activated ion channel, is required for vascular development in mice. Proceedings of the National Academy of Sciences of the United States of America 111: 10347-10352. DOI: 10.1073/pnas.1409233111.

Rezende LFMD, Sá THD, Markozannes G, Rey-López JP, Lee IM, Tsilidis KK, Ioannidis JPA, Eluf-Neto J (2018) Physical activity and cancer: an umbrella review of the literature including 22 major anatomical sites and 770 000 cancer cases. British Journal of Sports Medicine 52: 826-833. DOI: 10.1136/bjsports-2017-098391.

Servin-Vences MR, Moroni M, Lewin GR, Poole K (2017) Direct measurement of TRPV4 and PIEZO1 activity reveals multiple mechanotransduction pathways in chondrocytes. eLife 6: e21074. DOI: 10.7554/eLife.21074.

Shin KC, Park HJ, Kim JG, Lee IH, Cho H, Park C, Sung TS, Koh SD, Park SW, Bae YM (2019) The Piezo2 ion channel is mechanically activated by low-threshold positive pressure. Scientific Reports 9: 6446. DOI: 10.1038/s41598-019-42492-4.

Stamatakis E, Ahmadi MN, Gill JMR, Thøgersen-Ntoumani C, Gibala MJ, Doherty A, Hamer M (2022) Association of wearable device-measured vigorous intermittent lifestyle physical activity with mortality. Nature Medicine 28: 2521-2529. DOI: 10.1038/s41591-022-02100-x.

Stamatakis E, Huang BH, Maher C, Thøgersen-Ntoumani C, Stathi A, Dempsey PC, Johnson N, Holtermann A, Chau JY, Sherrington C, Daley AJ, Hamer M, Murphy MH, Tudor-Locke C, Gibala MJ (2021) Untapping the Health Enhancing Potential of Vigorous Intermittent Lifestyle Physical Activity (VILPA): Rationale, Scoping Review, and a 4-Pillar Research Framework. Sports Medicine (Auckland, N.Z.) 51: 1-10. DOI: 10.1007/s40279-020-01368-8.

Stamatakis E, Johnson NA, Powell L, Hamer M, Rangul V, Holtermann A (2019) Short and sporadic bouts in the 2018 US physical activity guidelines: is high-intensity incidental physical activity the new HIIT? British Journal of Sports Medicine 53: 1137-1139. DOI: 10.1136/bjsports-2018-100397.

Suchyna TM, Tape SE, Koeppe RE, 2nd, Andersen OS, Sachs F, Gottlieb PA (2004) Bilayer-dependent inhibition of mechanosensitive channels by neuroactive peptide enantiomers. Nature 430: 235-240. DOI: 10.1038/nature02743.

Syeda R, Xu J, Dubin AE, Coste B, Mathur J, Huynh T, Matzen J, Lao J, Tully DC, Engels IH, Petrassi HM, Schumacher AM, Montal M, Bandell M, Patapoutian A (2015) Chemical activation of the mechanotransduction channel Piezo1. eLife 4: e07369. DOI: 10.7554/eLife.07369.

Tsuchiya M, Hara Y, Okuda M, Itoh K, Nishioka R, Shiomi A, Nagao K, Mori M, Mori Y, Ikenouchi J, Suzuki R, Tanaka M, Ohwada T, Aoki J, Kanagawa M, Toda T, Nagata Y, Matsuda R, Takayama Y, Tominaga M, Umeda M (2018) Cell surface flip-flop of phosphatidylserine is critical for PIEZO1-mediated myotube formation. Nature Communications 9: 2049. DOI: 10.1038/s41467-018-04436-w.

Valdivia A, Avalos AM, Leyton L (2023) Thy-1 (CD90)-regulated cell adhesion and migration of mesenchymal cells: insights into adhesomes, mechanical forces, and signaling pathways. Frontiers in Cell and Developmental Biology 11: 1221306. DOI: 10.3389/fcell.2023.1221306.

Verkest C, Schaefer I, Nees TA, Wang N, Jegelka JM, Taberner FJ, Lechner SG (2022) Intrinsically disordered intracellular domains control key features of the mechanically-gated ion channel PIEZO2. Nature Communications 13: 1365. DOI: 10.1038/s41467-022-28974-6.

Wang L, Wang X, Ji N, Li HM, Cai SX (2020) Mechanisms of the mechanically activated ion channel Piezo1 protein in mediating osteogenic differentiation of periodontal ligament stem cells via the Notch signaling pathway. Hua Xi Kou Qiang Yi Xue Za Zhi = Huaxi Kouqiang Yixue Zazhi = West China Journal of Stomatology 38: 628-636. DOI: 10.7518/hxkq.2020.06.004. (In Chinese)

Wang Z, Chen J, Babicheva A, Jain PP, Rodriguez M, Ayon RJ, Ravellette KS, Wu L, Balistrieri F, Tang H, Wu X, Zhao T, Black SM, Desai AA, Garcia JGN, Sun X, Shyy JYJ, Valdez-Jasso D, Thistlethwaite PA, Makino A, Wang J, Yuan JXJ (2021) Endothelial upregulation of mechanosensitive channel Piezo1 in pulmonary hypertension. American Journal of Physiology. Cell Physiology 321: C1010-C1027. DOI: 10.1152/ajpcell.00147.2021.

Wijerathne TD, Ozkan AD, Lacroix JJ (2022) Yoda1's energetic footprint on Piezo1 channels and its modulation by voltage and temperature. Proceedings of the National Academy of Sciences of the United States of America 119: e2202269119. DOI: 10.1073/pnas.2202269119.

Wijerathne TD, Ozkan AD, Lacroix JJ (2023) Microscopic mechanism of PIEZO1 activation by pressure-induced membrane stretch. The Journal of General Physiology 155: e202213260. DOI: 10.1085/jgp.202213260.

Wong TY, Juang WC, Tsai CT, Tseng CJ, Lee WH, Chang SN, Cheng PW (2018) Mechanical Stretching Simulates Cardiac Physiology and Pathology through Mechanosensor Piezo1. Journal of Clinical Medicine 7: 410. DOI: 10.3390/jcm7110410.

Wu J, Young M, Lewis AH, Martfeld AN, Kalmeta B, Grandl J (2017) Inactivation of Mechanically Activated Piezo1 Ion Channels Is Determined by the C-Terminal Extracellular Domain and the Inner Pore Helix. Cell Reports 21: 2357-2366. DOI: 10.1016/j.celrep.2017.10.120.

Yang D, Wei GY, Li M, Peng MS, Sun Y, Zhang YL, Lu C, Qing KX, Cai HB (2021) Cyclic tensile strain facilitates proliferation and migration of human aortic smooth muscle cells and reduces their apoptosis via miRNA-187-3p. Bioengineered 12: 11439-11450. DOI: 10.1080/21655979.2021.2009321.

Yang F, Xiao X, Lee BH, Vu S, Yang W, Yarov-Yarovoy V, Zheng J (2018) The conformational wave in capsaicin activation of transient receptor potential vanilloid 1 ion channel. Nature Communications 9: 2879. DOI: 10.1038/s41467-018-05339-6.

Yang X, Lin C, Chen X, Li S, Li X, Xiao B (2022) Structure deformation and curvature sensing of PIEZO1 in lipid membranes. Nature 604: 377-383. DOI: 10.1038/s41586-022-04574-8.

Zhang P, Liu X, Guo P, Li X, He Z, Li Z, Stoddart MJ, Grad S, Tian W, Chen D, Zou X, Zhou Z, Liu S (2021) Effect of cyclic mechanical loading on immunoinflammatory microenvironment in biofabricating hydroxyapatite scaffold for bone regeneration. Bioactive Materials 6: 3097-3108. DOI: 10.1016/j.bioactmat.2021.02.024.

Zhao Q, Zhou H, Chi S, Wang Y, Wang J, Geng J, Wu K, Liu W, Zhang T, Dong MQ, Wang J, Li X, Xiao B (2018) Structure and mechanogating mechanism of the Piezo1 channel. Nature 554: 487-492. DOI: 10.1038/nature25743.

Zheng W, Gracheva EO, Bagriantsev SN (2019) A hydrophobic gate in the inner pore helix is the major determinant of inactivation in mechanosensitive Piezo channels. eLife 8: e44003. DOI: 10.7554/eLife.44003.

Zhou T, Gao B, Fan Y, Liu Y, Feng S, Cong Q, Zhang X, Zhou Y, Yadav PS, Lin J, Wu N, Zhao L, Huang D, Zhou S, Su P, Yang Y (2020) Piezo1/2 mediate mechanotransduction essential for bone formation through concerted activation of NFAT-YAP1-ß-catenin. eLife 9: e52779. DOI: 10.7554/eLife.52779.

Zhu Z, Tang T, He Z, Wang F, Chen H, Chen G, Zhou J, Liu S, Wang J, Tian W, Chen D, Wu X, Liu X, Zhou Z, Liu S (2023) Uniaxial cyclic stretch enhances osteogenic differentiation of OPLL-derived primary cells via YAP-Wnt/$\beta$-catenin axis. European Cells & Materials 45: 31-45. DOI: 10.22203/eCM.v045a03.

**Editor's note**: The Scientific Editor responsible for this paper was Chris Evans.